Original Article

Comparison of virtual and true non-contrast images from dual-layer spectral detector computed tomography (CT) in patients with colorectal cancer

Deying Wen[1#^], Qian Pu[1#], Pengfei Peng[1], Xun Yue[1,2], Yue Ming[1], Huiyi Yang[1], Jianyang Yang[3], Xiaodi Zhang[4], Haiwei Liu[5], Lie Yang[3], Jiayu Sun[1^]

[1]Department of Radiology, West China Hospital, Sichuan University, Chengdu, China; [2]Department of Radiology, Affiliated Hospital of North Sichuan Medical College, Nanchong, China; [3]Division of Gastrointestinal Surgery, Department of General Surgery, West China Hospital, Sichuan University, Chengdu, China; [4]Clinical Science, Philips Healthcare, Chengdu, China; [5]Advanced Clinical Application, Philips Healthcare, Beijing, China

Contributions: (I) Conception and design: J Sun, L Yang, D Wen, Q Pu; (II) Administrative support: J Sun, L Yang; (III) Provision of study materials or patients: P Peng, X Yue; (IV) Collection and assembly of data: H Yang, Y Ming; (V) Data analysis and interpretation: D Wen, Q Pu, X Zhang; (VI) Manuscript writing: All authors; (VII) Final approval of manuscript: All authors.

[#]These authors contributed equally to this work.

Correspondence to: Lie Yang, MD. Division of Gastrointestinal Surgery, Department of General Surgery, West China Hospital, Sichuan University, Guoxue Xiang No. 37, Chengdu 610041, China. Email: lie_222@163.com; Jiayu Sun, MD. Department of Radiology, West China Hospital, Sichuan University, Guoxue Xiang No. 37, Chengdu 610041, China. Email: cardiac_wchscu@163.com.

Background: Colorectal cancer (CRC) is commonly assessed by computed tomography (CT), but the associated radiation exposure is a major concern. This study aimed to quantitatively and qualitatively compare the image quality of virtual non-contrast (VNC) images reconstructed from arterial and portal venous phases with that of true non-contrast (TNC) images in patients with CRC to assess the potential of TNC images to replace VNC images, thereby reducing the radiation dose.

Methods: A total of 69 patients with postoperative pathologically confirmed CRC at the West China Hospital of Sichuan University between May 2022 and April 2023 were enrolled in this cross-sectional study. The CT protocol included the acquisition of TNC images, arterial and portal venous phase images; the VNC images were reconstructed from the two postcontrast phase images. Several parameters, including the CT attenuation value, absolute attenuation error, imaging noise [standard deviation (SD)], signal-to-noise ratio (SNR), and contrast-to-noise ratio (CNR), were measured in multiple abdominal structures for both the TNC and VNC images. Two blinded readers assessed the subjective image quality using a five-point scale. Interobserver agreement was evaluated using interclass correlation coefficients (ICCs). The paired t-test and Wilcoxon signed-rank test were used to compare the objective and subjective results between the TNC and VNC images. Individual measurements of radiation doses for the TNC scan and contrast scan protocols were recorded.

Results: A total of 2,070 regions of interest (ROIs) of the 69 patients were analyzed. Overall, the VNC images exhibited significantly lower attenuation values and SD values than the TNC images in all tissues, except for the abdominal aorta, portal vein, and spleen. The mean absolute attenuation errors between the VNC and TNC images were all less than 10 Hounsfield units (HU). The percentages of absolute attenuation errors less than 5 and 10 HU in the VNC images from the arterial phase (VNCa) were 78.99% and 97.97%, respectively, while those from the portal venous phase (VNCp) were 81.59% and 96.96%, respectively. The

^ ORCID: Deying Wen, 0000-0003-0866-1607; Jiayu Sun, 0000-0002-0920-5948.

absolute attenuation errors between the TNC and VNCa images were smaller than those between the TNC and VNCp images for tumors [VNCaerror: 2.77, interquartile range (IQR) 1.77–4.22; VNCperror: 3.27, IQR 2.68–4.30; P=0.002]. The SNR values and CNR values in the VNC images were significantly higher than those in the TNC images for all tissues, except for the portal vein and spleen. The image quality was rated as excellent (represented by a score of 5) in the majority of the TNC and VNC images; however, the VNC images scored lower than the TNC images. Eliminating the TNC phase resulted in a reduction of approximately 37.99% in the effective dose (ED).

Conclusions: The VNC images provided accurate CT attenuation, good image quality, and lower radiation doses than the TNC images in CRC, and the VNCa images showed minimal differences in the CT attenuation of the tumors.

Keywords: Colorectal cancer (CRC); dual-layer detector spectral computed tomography (dual-layer detector spectral CT); virtual non-contrast (VNC); image quality; radiation dose

Submitted Mar 16, 2024. Accepted for publication Aug 05, 2024. Published online Aug 28, 2024.
doi: 10.21037/qims-24-535
View this article at: https://dx.doi.org/10.21037/qims-24-535

Introduction

Colorectal cancer (CRC) is a common malignancy of the digestive system, and is the second leading cause of cancer-related death worldwide (1,2). Due to its high spatial resolution, computed tomography (CT) is a widely used clinical imaging method for evaluating CRC (3-9). It plays a critical role in various aspects of CRC evaluations, including screening, diagnosis, preoperative staging, and treatment response assessment. However, the radiation exposure associated with CT scans is a significant concern, particularly for CRC patients who often require multiple follow-up scans. In clinical practice, a common CT scanning approach for patients with CRC involves a combination of non-contrast and contrast-enhanced CT scans. While effective, this approach may subject patients to higher radiation doses as a result.

Dual-layer spectral detector computed tomography (SDCT) is an advanced imaging technology that uses a dual-layer detector. It simultaneously acquires high- and low-energy information during routine scans, enabling the generation of spectral-based imaging (SBI), which can be directly used to realize the reconstruction of spectral multiparameter images for retrospective analysis. Using SDCT, virtual non-contrast (VNC) images can be reconstructed from contrast-enhanced scans by subtracting iodine attenuation from the contrast data. This process results in images that closely resemble conventional plain scans [i.e., true non-contrast (TNC) scans], effectively replacing the need for separate TNC scans and reducing patient radiation exposure (10-13). VNC imaging has been widely used in various anatomical regions, including the head (10), neck (11), spine (12), and abdomen (13-16). Comparative studies of VNC and TNC images have shown the value of VNC images in abdominal imaging for non-traumatic acute abdomen or aortic aneurysms (17), renal carcinoma (18,19), and fatty liver disease (20).

To our knowledge, few studies have explored the feasibility of using VNC images, reconstructed from multi-phase enhancement images, as a substitute for TNC images in patients with CRC. This study sought to address this gap by conducting a comprehensive quantitative and qualitative comparison of the image quality of VNC images reconstructed from both the arterial phase and portal venous phase to that of traditional TNC images in patients diagnosed with CRC. Additionally, the study evaluated whether radiation exposure could be reduced by eliminating the TNC phase from the scanning protocol. We present this article in accordance with the STROBE reporting checklist (available at https://qims.amegroups.com/article/view/10.21037/qims-24-535/rc).

Methods

Study population

The study was conducted in accordance with the Declaration of Helsinki (as revised in 2013), and was approved by the Biomedical Ethics Committee of West China Hospital, Sichuan University (No. 2022 1904). All

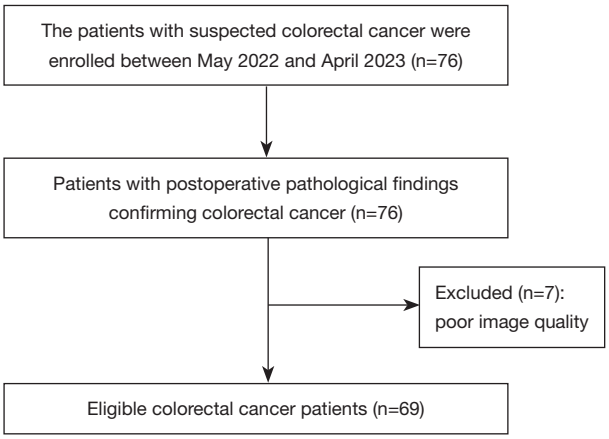

Figure 1 Patient selection flowchart.

the participating patients provided informed consent before undergoing the examination.

A total of 69 patients (44 male and 25 female) presenting for their initial consultation at West China Hospital of Sichuan University were enrolled in the study. The patients had a mean age of 61.36±13.0 years (range, 25 to 84 years). To be eligible for inclusion in this study, the CRC patients had to meet the following inclusion criteria: (I) have a confirmed diagnosis of CRC based on postoperative pathological findings; (II) have undergone a pre-surgery thoracoabdominal CT examination, which included TNC scans and contrast-enhanced arterial and portal venous scans performed before surgery; and (III) be aged 18 years or older. Patients were excluded from the study due to poor image quality and un-assessable images resulting from significant respiratory motion artifacts. The patient recruitment period spanned from May 2022 to April 2023. The screening processes for the patients are shown in *Figure 1*.

CT scanning protocol

Prior to the CT scan, all patients were instructed to follow a low-fat, low-fiber, low-residue, or liquid diet for two days. Additionally, they were required to fast for four to six hours before the examination and ingest 200 mL of drinking water immediately before the CT scan. All patients underwent triphasic thoracoabdominal CT scans (including TNC and contrast-enhanced arterial and portal venous scans) in a supine position using a dual-layer spectral detector CT machine (Spectral CT 7500; Philips Healthcare, Amsterdam, The Netherlands). The imaging procedure began with an anteroposterior scout scan, followed by a pre-contrast phase that covered the region from the upper edge of the lung to the lower edge of the pubic symphysis. Subsequently, an intravenous contrast agent with a total amount of 1.2–1.5 mL/kg of body weight was administered at a flow rate of 3–5 mL/s using a high-pressure injector system. A bolus tracking method was employed, with a threshold value set at 150 Hounsfield units (HU) in the abdominal aorta. The arterial scan was automatically triggered when the contrast agent reached its peak concentration, while the portal venous scan was initiated 70 seconds after the injection of the contrast agent. The postcontrast scans encompassed the region from the upper edge of the liver to the lower edge of the pubic symphysis. All the acquired datasets were reconstructed into axial images with a slice thickness and interval of 1 mm. The scanning parameters were as follows: tube voltage: 120 kVp; tube current: modulated using automated exposure control; pitch: 1.000; rotation time: 0.5 seconds; collimation: 128×0.625 mm; field of view: 350 mm × 350 mm; matrix: 512×512; and filter: standard (B). The conventional images were reconstructed using the iDose 4 algorithm, and the SBI scans were reconstructed using the spectral level 4 algorithm.

Image reconstruction

Both conventional CT and spectral-based images were generated, after which the SBI scans were transferred to a dedicated spectral post-processing workstation (IntelliSpace Portal; Philips Healthcare, Amsterdam, The Netherlands). Subsequently, the VNC images were reconstructed from both the arterial and portal venous phases for each patient. The section thickness and the increment for these images were set at 1 mm.

Image analysis—objective evaluation

The CT attenuation and standard deviation (SD) measurements were performed on several representative regions of interest (ROIs) in both the TNC and VNC images, which were reconstructed from the arterial and portal venous phases. These assessments were performed by two independent observers. The first observer was an expert with 10 years of experience in abdominal imaging, and the second observer was a master's degree student specializing in medical imaging. The selected ROIs comprised various areas, including the colorectal tumor, normal colorectal

tissue, abdominal aorta, muscle (specifically, the psoas muscle in patients with colon cancer, and the gluteal muscle in patients with rectal cancer), subcutaneous fat, liver, portal vein, spleen, and renal cortex. To ensure consistent and reliable measurements, specific criteria were applied when placing the ROIs. For instance, the ROIs for the tumors, liver, spleen, and kidneys were positioned at the largest imaging level to avoid regions with liquefaction, necrosis, calcification, or blood vessels. The ROIs for the muscle and subcutaneous fat were placed at the same imaging level as the tumor to ensure consistency. Circular ROIs were initially placed on images from the arterial or portal venous phase images, and then copied onto the TNC and VNC images. The circular ROIs used were approximately 100 mm^2 in size, but if the tissue being measured was smaller than 100 mm^2, the ROI was adjusted to cover the entire area. However, in the case of the renal cortex, an oval-shaped ROI was employed to adequately cover the cortical area. The size of the tumor ROI was tailored to the tumor's overall dimensions to ensure a precise depiction. To account for potential discrepancies caused by patient breathing and movement, manual adjustments were made to align the ROIs accurately. In total, 2,070 ROIs were measured (10 ROIs for each of the three phases in 69 patients). Each ROI was measured three times, on the largest plane and its two adjacent planes, and the average of the three measurements was taken as the result for each observer. Subsequently, the average measurements from both observers were used to calculate the final values for each ROI. A schematic diagram of the ROIs is provided in *Figure 2*.

After obtaining the CT attenuation and SD values, the absolute attenuation error, which represents the accuracy of the CT attenuation (13), and the signal-to-noise ratio (SNR) and contrast-to-noise ratio (CNR), which represent the quality of the image, were further calculated using the following formulas:

$$VNCa_{error} = \left| HU_{VNCa} - HU_{TNC} \right| \quad [1]$$

where $VNCa_{error}$ refers to the absolute attenuation error between the virtual non-contrast image from the arterial phase (VNCa) and the TNC image, HU_{VNCa} refers to the CT attenuation of the VNCa images, and HU_{TNC} refers to the CT attenuation of the TNC images;

$$VNCp_{error} = \left| HU_{VNCp} - HU_{TNC} \right| \quad [2]$$

where $VNCp_{error}$ refers to the absolute attenuation error between the virtual non-contrast image from the portal venous phase (VNCp) and the TNC image, and HU_{VNCp} refers to the CT attenuation of the VNCp images.

An absolute attenuation error between the VNC and TNC images of 10 HU or less was considered acceptable (15,21).

The formula for the SNR is expressed as follows:

$$SNR = HU_{ROI} / SD_{ROI} \quad [3]$$

where HU_{ROI} refers to the CT attenuation of the ROI, and SD_{ROI} refers to the SD of the ROI.

The formula for the CNR is expressed as follows:

$$CNR = \left(HU_{ROI} - HU_{muscle} \right) / SD_{muscle} \quad [4]$$

where HU_{ROI} refers to the CT attenuation of the ROI, HU_{muscle} refers to the CT attenuation of muscle, and SD_{muscle} refers to the SD of the muscle.

Image analysis—subjective evaluation

The subjective assessment of the images was performed by two additional independent readers, each with 15 years of experience in interpreting abdominal images. These readers were unaware of the specific image reconstructions being evaluated. The images were scored on a five-point grade scale (22) based on several factors, including the display of the anatomical details, the presence of artifacts, and the level of image noise. The grading scale was as follows: 5 = excellent, 4 = good, 3 = moderate, 2 = poor, and 1 = non-diagnostic.

Radiation dose evaluation

The dose-length product (DLP, mGy·cm) and effective dose (ED, mSv) values were recorded for all patients in the TNC scan and contrast scan protocols. The ED was calculated from the DLP registered by the CT scanner and multiplied by a conversion coefficient (k) valued at 0.015 mSv/(mGy·cm) (20,23), thereby yielding the following formula: ED = k × DLP, where k is set at 0.015.

Statistical analysis

The distribution of the variables was assessed using the Shapiro-Wilk test. The normally distributed data are expressed as the mean ± SD, and the non-normally distributed data are expressed as the median and interquartile range (IQR). As our evaluators were specifically selected and not randomly selected, we

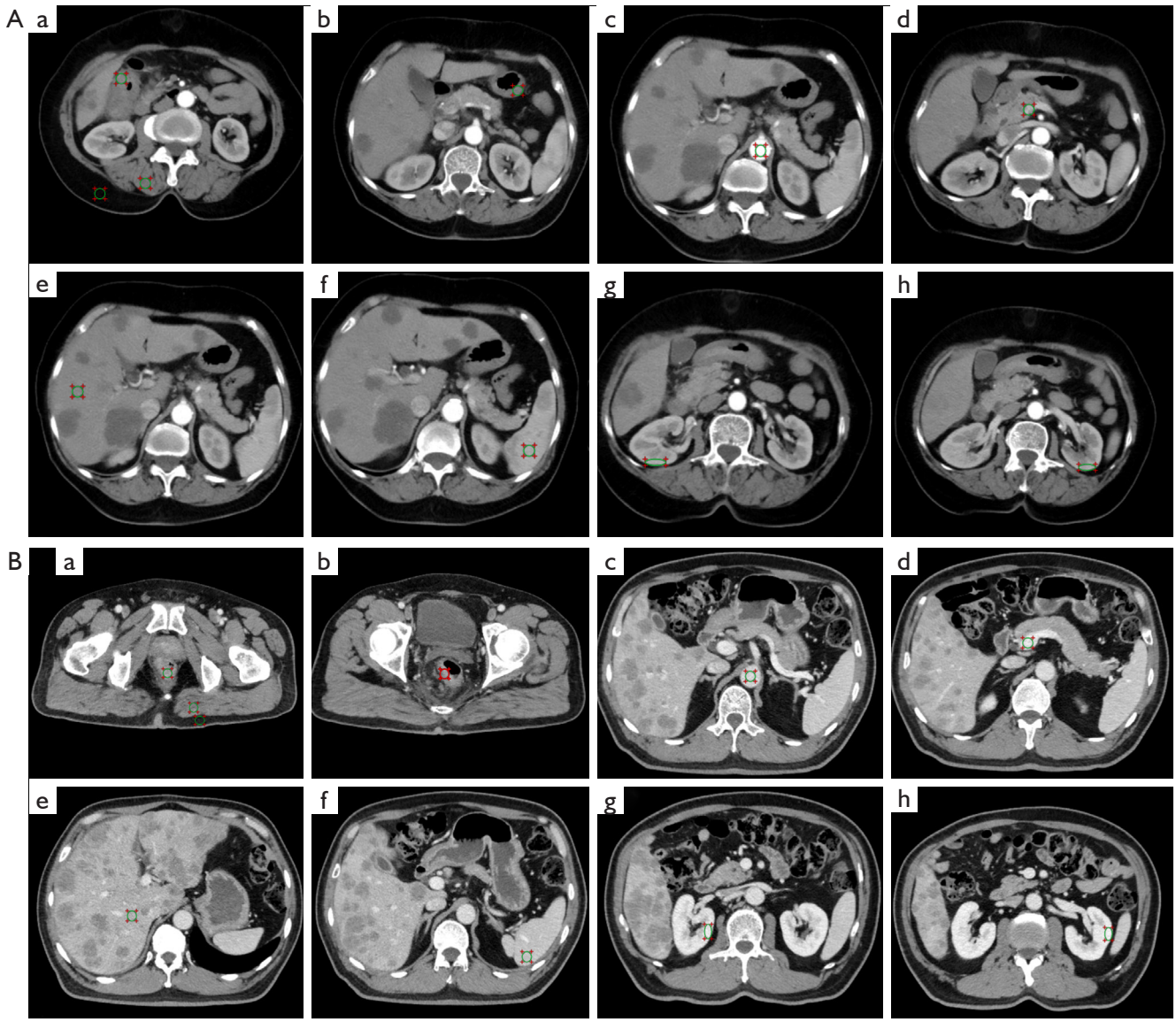

Figure 2 Illustrations of the ROIs in colorectal, (A) colon, and (B) rectal tumors. The circular ROIs, initially positioned on images from either the arterial or portal venous phase, were subsequently replicated onto the TNC and VNC phase images. (a) Tumor, muscle and subcutaneous fat; (b) normal colorectal tissue; (c) abdominal aorta; (d) portal vein; (e) liver; (f) spleen; (g) right renal cortex; (h) left renal cortex. ROIs, regions of interest; TNC, true non-contrast; VNC, virtual non-contrast.

employed the interclass correlation coefficient (ICC) (type 3) to evaluate interobserver agreement across all measurements and assessments. The interobserver agreement was interpreted as follows: poor: 0≤ ICC ≤0.2; fair: 0.2< ICC ≤0.4; moderate: 0.4< ICC ≤0.6; good: 0.6< ICC ≤0.8; and excellent: 0.8< ICC ≤1.0.

The objective assessments, including the CT attenuation, SD, SNR, and CNR values, were compared between the TNC and VNC images using the paired *t*-test and Wilcoxon signed-rank test. A Bland-Altman analysis was used to evaluate the measurement agreement between the mean CT attenuation on the TNC images and VNC images. The Wilcoxon signed-rank test was used to compare the subjective evaluation of the TNC and VNC image quality.

The statistical analyses were conducted using SPSS 25.0 (IBM, Corp., Armonk, NY, USA) and MedCalc (version 20.218) statistical software. A P value <0.05 (two-

Table 1 Demographic and clinical characteristics of patients

Characteristics	Value
Sex	
Male	44 (63.77)
Female	25 (36.23)
Age (years)	61.36±13.0
Location of lesion	
Colon	17 (24.64)
Rectum	52 (75.36)

Data are expressed as the mean ± standard deviation or n (%).

sided) was considered statistically significant.

Results

Patient characteristics

A total of 69 patients were enrolled in this study, of whom 44 were male, and 25 were female. The patients had a mean age of 61.36±13.0 years. All the patients had confirmed postoperative pathology reports of CRC; 17 patients had colonic lesions, and 52 patients had rectal lesions. Detailed patient characteristics are presented in *Table 1*.

Interobserver agreement

Interobserver agreement between the two observers was assessed for all measurements of the 69 participants, yielding excellent results with all ICC values exceeding 0.80. A summary of the interobserver agreement results can be found in Table S1.

Comparison of VNCa and TNC images

In the comparison of the VNCa and TNC images, the CT attenuation values in all tissues were significantly lower in the VNCa images, except for the abdominal aorta, which exhibited higher CT attenuation values in the VNCa images (P<0.001). Additionally, the SD values were significantly lower in the VNCa images across all tissues (P<0.001). The SNR and CNR values were higher in the VNCa images than the TNC images (P<0.05), except for the portal vein, which displayed a lower CNR value in the VNCa images. Detailed objective evaluation results are provided in Tables S2,S3. *Figure 3* provides an example of the differences in the CT numbers observed in tumors.

Comparison of VNCp and TNC images

The VNCp images were compared to the TNC images, and while no statistically significant difference was found in the CT attenuation values for the portal vein, in other tissues, the values of the VNCp images exhibited significantly lower CT attenuation values (P<0.001). The SD values of the VNCp images were lower than those of the TNC images across all tissues, except for the spleen. The SNR and CNR values of the VNCp images were higher than those of the TNC images (P<0.05) in all tissues, except for the spleen. Detailed results for the objective evaluation indicators are provided in Tables S2,S3.

Comparison of VNCa and VNCp images

The comparison of the VNCa and VNCp images showed that the CT attenuation values of the VNCa images were higher than those of the VNCp images in the normal colorectum, muscle, portal vein, and spleen. Conversely, the VNCa images had significantly lower CT attenuation values in the other ROIs (P<0.05). The SD values of the VNCp images were higher than those of the VNCa images in the normal colorectum, muscle, portal vein, liver, and spleen (P<0.001). The SNRs of the VNCa images were higher than those of the VNCp images (P<0.05) in all tissues, except for the abdominal aorta, left kidney, and subcutaneous fat. Conversely, the SNRs of the VNCp images were higher than those of the VNCa images in the subcutaneous fat (P<0.001). The CNRs of the VNCa images were higher than those of the VNCp images (P<0.05) in the subcutaneous fat, abdominal aorta, liver, and spleen (P<0.001). For further details, see Tables S2,S3.

Absolute attenuation error between TNC and VNC images

The mean absolute attenuation errors of the VNC images were consistently less than 10 HU. The largest and smallest absolute attenuation errors of the VNC images were observed in the subcutaneous fat (VNCp: 6.83, IQR 4.30–9.67 and VNCa: 5.83, IQR 3.25–8.60) and the portal vein (VNCa: 1.46, IQR 0.80–3.05 and VNCp: 1.43, IQR 1.03–2.35), respectively. Significant differences in the absolute attenuation errors were found between the VNCa images and VNCp images for all tissues, except for the portal vein. The absolute attenuation errors between the TNC and

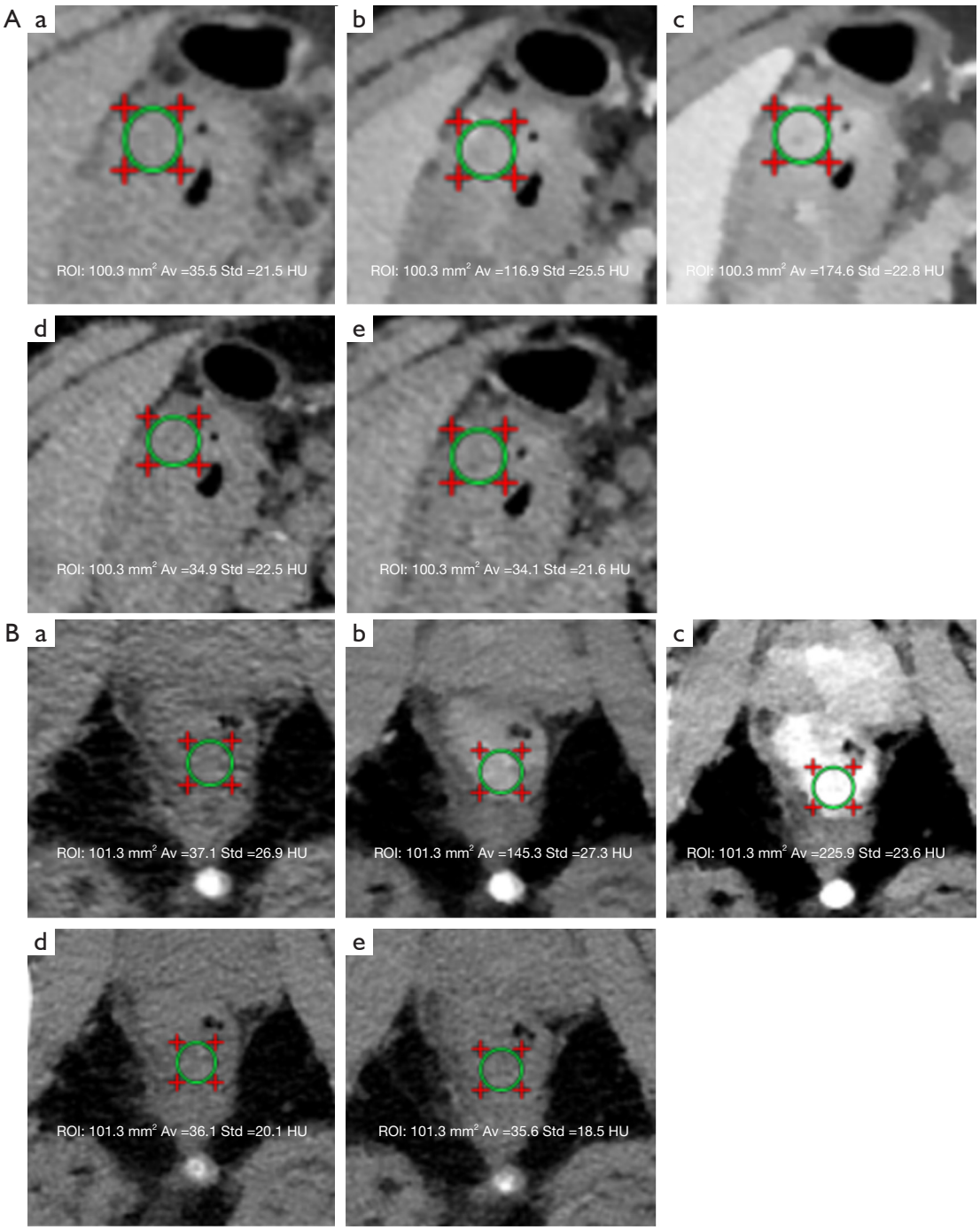

Figure 3 Images showing differences in CT numbers in the region of the colorectal tumor [(A) colon tumor; (B) rectal tumor]. (a-e) The TNC, arterial phase, portal venous phase, VNCa, and VNCp images, respectively. ROI, region of interest; Av, average; Std, standard deviation; CT, computed tomography; TNC, true non-contrast; VNCa, virtual non-contrast image from the arterial phase; VNCp, virtual non-contrast image from the portal venous phase; HU, Hounsfield units.

Table 2 Mean absolute attenuation errors between the TNC and VNC images

Region	$VNCa_{error}$ (HU)	$VNCp_{error}$ (HU)	P*
Tumor	2.77 (1.77–4.22)	3.27 (2.68–4.30)	0.002
Normal colorectum	2.93±1.79	3.10 (1.88–4.75)	0.004
Muscle	3.88±1.56	2.73 (2.02–3.57)	<0.001
Subcutaneous fat	5.83 (3.25–8.60)	6.83 (4.30–9.67)	<0.001
Abdominal aorta	4.87 (3.78–7.10)	3.23 (1.83–4.43)	<0.001
Portal vein	1.46 (0.80-3.05)	1.43 (1.03–2.35)	0.522
Liver	3.03 (2.25–4.22)	2.37 (1.37–4.40)	0.004
Spleen	3.50±1.28	2.13 (1.47–2.97)	<0.001
Renal cortex-L	2.83 (1.40–4.05)	3.42±1.82	0.009
Renal cortex-R	1.67 (1.15–2.80)	2.59±1.24	<0.001

Data are expressed as the mean ± standard deviation or median (interquartile range). *, comparison of $VNCa_{error}$ and $VNCp_{error}$. TNC, true non-contrast; VNC, virtual non-contrast; $VNCa_{error}$, the absolute attenuation error between VNCa and TNC images; $VNCp_{error}$, the absolute attenuation error between VNCp and TNC images; VNCa, virtual non-contrast image from the arterial phase; HU, Hounsfield unit; VNCp, virtual non-contrast image from the portal venous phase; Renal cortex-L, left renal cortex; Renal cortex-R, right renal cortex.

VNCa images were smaller than those between the TNC and VNCp images for tumors. A comprehensive summary of the absolute attenuation errors for the VNC images across all the evaluated tissues is presented in *Table 2*.

Overall, the percentages of the VNC images with absolute attenuation errors less than 5 and 10 HU in the arterial phase CT were 78.99% and 97.97%, respectively, and those in the portal venous phase CT were 81.59% and 96.96%, respectively. Further details on the absolute attenuation errors less than 5 and 10 HU are provided in *Table 3*. Bland-Altman plots illustrating the measurement agreement between the CT attenuation on the TNC images and VNC images in all regions can be found in Figure S1.

Subjective assessment

The scores assigned by both readers to the TNC images [5 (IQR 5–5)] were significantly higher than those for the VNCa [5 (IQR 4–5)] and VNCp [5 (IQR 4–5)] images (P<0.05). No significant differences were observed in the scores between the VNCa and VNCp images for either reader (P>0.05). Image quality was rated as excellent (a score of 5) in the majority of the TNC, VNCa, and VNCp images with slight variations between the two readers. All the images received scores above three on the five-point scale. For a detailed evaluation of the image quality, see *Table 4*.

Radiation dose evaluation

The ED values for the CT scan, including all scanned phases, were 32.87±7.16 mSv. In the contrast CT scan, excluding the TNC scan, the ED value was 20.38±4.49 mSv. Thus, eliminating the TNC phase resulted in an ED reduction of approximately 37.99%.

Discussion

In the current investigation, we conducted a comprehensive examination of objective image quality parameters, including CT attenuation, image noise, the SNR, the CNR, and the absolute attenuation error, as well as an assessment of the subjective image quality of VNC images obtained from arterial and portal venous phase scans using a dual-layer spectral detector CT system. Our findings revealed a high degree of concordance between the VNC and TNC images in CRC and other abdominal tissues. Notably, we observed that the image quality was consistently favorable in both the VNC and TNC images, leading to a significant reduction in the effective radiation dose, which was reduced by approximately 37.99% when the TNC scans were omitted.

In our investigation, we found statistically significant differences in the CT attenuation values between the VNC and TNC images, which were significantly lower than the

Table 3 Absolute attenuation errors less than 5 and 10 HU

Region	$VNCa_{error}$, n (%)		$VNCp_{error}$, n (%)	
	<5 HU	<10 HU	<5 HU	<10 HU
Tumor	56 (81.16)	69 (100.00)	57 (82.61)	67 (97.10)
Normal colorectum	60 (86.96)	69 (100.00)	54 (78.26)	68 (98.55)
Muscle	53 (76.81)	69 (100.00)	64 (92.75)	68 (98.55)
Subcutaneous fat	27 (39.13)	59 (85.51)	22 (31.88)	55 (79.71)
Abdominal aorta	36 (52.17)	65 (94.20)	57 (82.61)	67 (97.10)
Portal vein	68 (98.55)	69 (100.00)	68 (98.55)	69 (100.00)
Liver	57 (82.61)	69 (100.00)	56 (81.16)	68 (98.55)
Spleen	61 (88.41)	69 (100.00)	63 (91.30)	69 (100.00)
Renal cortex-L	59 (85.51)	69 (100.00)	56 (81.16)	69 (100.00)
Renal cortex-R	68 (98.55)	69 (100.00)	66 (95.65)	69 (100.00)
Total (%)	78.99	97.97	81.59	96.96

HU, Hounsfield units; $VNCa_{error}$, the absolute attenuation error between VNCa and TNC images; $VNCp_{error}$, the absolute attenuation error between VNCp and TNC images; VNCa, virtual non-contrast image from the arterial phase; VNCp, virtual non-contrast image from the portal venous phase; Renal cortex-L, left renal cortex; Renal cortex-R, right renal cortex.

Table 4 Subjective evaluation of image quality

Score	TNC	VNCa	VNCp	P value		
				TNC *vs*. VNCa	TNC *vs*. VNCp	VNCa *vs*. VNCp
Reader 1				0.007	0.002	0.694
Score						
1	0	0	0			
2	0	0	0			
3	0	2	0			
4	10	18	20			
5	59	49	49			
Median [IQR]	5 [5–5]	5 [4–5]	5 [4–5]			
Reader 2				<0.001	<0.001	0.705
Score						
1	0	0	0			
2	0	0	0			
3	0	1	0			
4	7	23	23			
5	62	45	46			
Median [IQR]	5 [5–5]	5 [4–5]	5 [4–5]			

TNC, true non-contrast; VNCa, virtual non-contrast image from the arterial phase; VNCp, virtual non-contrast image from the portal venous phase; IQR, interquartile range.

TNC images in most tissues, including the tumor, liver, spleen, kidneys, muscle, and subcutaneous fat. However, exceptions were observed in the abdominal artery (where the CT attenuation values in VNCa image were higher than those in TNC images), and portal vein (P>0.05). These findings are informative but somewhat inconsistent with certain previous studies (19,20,24-27). For example, Zhang *et al.* reported no differences in the CT attenuation values for the liver, spleen, and arteries between VNC and TNC images, which contrasts with our observations. Conversely, Zhang *et al.* found that the values for the kidneys, subcutaneous fat, and psoas muscle were lower in the VNC images than the TNC images (19), which aligns with our results. Similarly, Jing *et al.* found significantly lower mean CT attenuation values for the liver and spleen in VNC images compared to TNC images (20), which is consistent with our findings. Conversely, Ananthakrishnan *et al.* concluded that VNC images overestimated HU relative to unenhanced images (22). Additionally, Lennartz *et al.* found no significant difference between the TNC and VNCp images in the abdominal aorta with the VNCp images even showing higher CT attenuation values in the portal vein than the TNC images, a finding that differs from our observations (25). These disparities may stem from variations in the reconstruction algorithms, period phase selection for VNC image reconstruction, scanner specifications, and imaging protocols for VNC images. In our study, the CT attenuation values of the abdominal arteries were higher in the VNCa images than the TNC images, which might be explained by the fact that the concentration of iodine in the arterial phase of the abdominal aorta was too high to be completely removed, resulting in higher CT attenuation values in the VNCa images than the TNC images.

To mitigate these discrepancies, we introduced an absolute attenuation error criterion, deeming errors of 10 HU or less as acceptable (15,21). This approach effectively balanced the discrepancies between the TNC and VNC images in both positive and negative directions. Overall, our results indicated that the mean absolute attenuation errors for the VNC images across all tissues were below 10 HU, with 80.29% and 97.47% of the VNC images exhibiting absolute attenuation errors below 5 and 10 HU, respectively. These findings suggest a slight improvement in the attenuation accuracy of the VNC images in our study compared to previous studies. Ananthakrishnan *et al.* reported absolute attenuation differences below 5 and 10 HU in only 44.4% and 75.2%, respectively, of all measurements between the VNC and TNC images (22). Conversely, Jamali *et al.* observed differences below 10 HU in 92.3% of cases (28), while Mergen *et al.* reported absolute attenuation errors below 5 HU in 76% and below 10 HU in 95% of measurements between the VNC and TNC images (13). They suggested that these disparities might be due to variances in scanner characteristics.

As is well known, VNC reconstructions are generated by subtracting iodine content from contrast-enhanced scans to create images that resemble TNC images. This technique is particularly useful in dual-energy CT imaging (29). Different CT scanners may use different types of dual-energy technology, such as dual-source, rapid kVp switching, or dual-layer detector systems. Each technology has its own method of acquiring and processing data, which can affect the VNC image quality. Additionally, manufacturers often develop proprietary algorithms for material decomposition and VNC reconstructions. These algorithms may handle the subtraction process differently, leading to variability in the final VNC images. Further, the post-processing techniques and software used can also contribute to the differences in VNC images. Different smoothing filters, noise reduction algorithms, and other image enhancement tools can alter the appearance of VNC reconstructions. Further, accurate VNC reconstructions depend on the proper calibration of the CT scanner and the appropriate selection of scanning parameters. Any variations in calibration or settings can result in discrepancies in VNC images. We also postulate that scanning protocols and period phase selection for VNC image reconstruction may contribute to these variations; thus, further research needs to be conducted.

Notably, the largest absolute attenuation error between the VNC and TNC images in our study was detected in subcutaneous fat; a finding consistent with previous research (15,19). However, given the minimal iodine uptake in fat, the exact reason for this finding remains unclear. Further, our study found that only 2–3% of patients exhibited absolute attenuation errors exceeding 10 HU between the TNC and VNC images. Smaller absolute attenuation error values and lower percentages of absolute attenuation errors exceeding 10 HU indicate superior agreement in CT attenuation between VNC and the TNC images. Additionally, the Bland-Altman plots revealed favorable agreement for the CT attenuation between the TNC and VNC images.

Moreover, we observed that the noise (SD) in the VNC images was significantly lower than in the TNC images across nearly all tissues, except for the spleen (P>0.05). This

observation aligns with the findings of previous studies (15,19,24) and might be due to smoothing induced by the spectral reconstruction algorithm at level 4; however, a subtle granularity was noted (24). This might have contributed to the lower subjective ratings of the VNC images compared to the TNC images.

Assessing colorectal lesions, in addition to major abdominal organs and tissues, is crucial for determining the viability of employing VNC images as an alternative to TNC images in the follow-up evaluations of patients with CRC. Our findings indicated significantly lower CT attenuation values in the VNC images than the TNC images in tumors, while the mean absolute attenuation error remained below 5 HU, and the SD values in the VNC images were lower than those in the TNC images. Further, the CNR and SNR values were consistently higher in the VNC images than the TNC images. To determine the optimal phase for reconstructing VNC images with minimal differences, we also compared the VNCa and VNCp images. The absolute attenuation errors between the TNC and VNCa images were smaller than those between the TNC and VNCp images for the tumor, normal colorectum, fat, and kidney, which suggests that the VNCa images had higher accuracy in these tissues. Conversely, the VNCp images had greater accuracy in the muscle, liver, spleen, and abdominal artery, with no difference in the portal vein. Thus, we recommend that VNCa images be used as an alternative to TNC to evaluate CRC patients. However, this recommendation diverges from previous studies; for example, Lehti *et al.* suggested that VNCp images represent TNC scans more accurately than VNCa images (30). These differences might be related to tissue-specific characteristics regarding the absorption and excretion process of iodine contrast agents; thus, further research needs to be conducted. Regarding other abdominal organs, we advise a prudent choice of the reconstruction phase for VNC images. This decision should be informed by considering the particular organ under examination, in tandem with the insights gained from our research.

This study had several limitations. First, bone tissue was not included in our analysis due to the similar absorption properties shared between bone and iodine, which renders differentiation using spectral CT challenging. Second, fluid-containing organs were also not included in the tissues we measured; for example, the bladder and gallbladder were excluded from our measurements, as iodine uptake in these organs is virtually absent. Third, our study focused solely on a single scanner and did not encompass a comparative analysis of VNC images acquired from other spectral detector CT systems. Fourth, this study used conventional dose scanning and processed the spectral data to generate VNC images using a fixed reconstruction algorithm, spectral level 4; future research should seek to investigate the effects of low-dose scanning or different reconstruction algorithms on image quality. Further, the reproducibility of VNC attenuation values across different manufacturers warrants further investigation. Finally, it is important to acknowledge that our study was conducted at a single center; thus, validation in larger multicenter studies is required.

Conclusions

We found robust agreement between the VNC and TNC images in assessing the image quality of tumors and abdominal tissues in CRC patients. Notably, the VNCa images exhibited the smallest discrepancies in the CT attenuation values for tumors. In the future, the use of VNC images as a substitute for TNC images may significantly reduce radiation doses for CRC patients.

Acknowledgments

Funding: This study was supported by the Key Research and Development Projects of Sichuan Province (Grant No. 2020YFS0123).

Footnote

Reporting Checklist: The authors have completed the STROBE reporting checklist. Available at https://qims.amegroups.com/article/view/10.21037/qims-24-535/rc

Conflicts of Interest: All authors have completed the ICMJE uniform disclosure form (available at https://qims.amegroups.com/article/view/10.21037/qims-24-535/coif). X.Z. serves as a clinical scientist at Philips Healthcare, and as part of her role, she provides technical support to clients. H.L. is a clinical specialist at Philips Healthcare, where he provides technical support to clients. The other authors have no conflicts of interest to declare.

Ethical Statement: The authors are accountable for all aspects of the work in ensuring that questions related

to the accuracy or integrity of any part of the work are appropriately investigated and resolved. The study was conducted in accordance with the Declaration of Helsinki (as revised in 2013), and was approved by the Biomedical Ethics Committee of West China Hospital, Sichuan University (No. 2022 1904). All the participating patients provided informed consent before undergoing the examination.

References

1. Shaukat A, Levin TR. Current and future colorectal cancer screening strategies. Nat Rev Gastroenterol Hepatol 2022;19:521-31.
2. Keum N, Giovannucci E. Global burden of colorectal cancer: emerging trends, risk factors and prevention strategies. Nat Rev Gastroenterol Hepatol 2019;16:713-32.
3. Sha J, Chen J, Lv X, Liu S, Chen R, Zhang Z. Computed tomography colonography versus colonoscopy for detection of colorectal cancer: a diagnostic performance study. BMC Med Imaging 2020;20:51.
4. Karlsson N, Zackrisson S, Buchwald P. Computed Tomography Verified Prevalence of Incisional Hernia 1 Year Postoperatively after Colorectal Cancer Resection. Scand J Surg 2021;110:373-9.
5. Dou Y, Liu Y, Kong X, Yang S. T staging with functional and radiomics parameters of computed tomography in colorectal cancer patients. Medicine (Baltimore) 2022;101:e29244.
6. Keyl J, Hosch R, Berger A, Ester O, Greiner T, Bogner S, Treckmann J, Ting S, Schumacher B, Albers D, Markus P, Wiesweg M, Forsting M, Nensa F, Schuler M, Kasper S, Kleesiek J. Deep learning-based assessment of body composition and liver tumour burden for survival modelling in advanced colorectal cancer. J Cachexia Sarcopenia Muscle 2023;14:545-52.
7. Klassen P, Baracos V, Gramlich L, Nelson G, Mazurak V, Martin L. Computed-Tomography Body Composition Analysis Complements Pre-Operative Nutrition Screening in Colorectal Cancer Patients on an Enhanced Recovery after Surgery Pathway. Nutrients 2020;12:3745.
8. Brown JC, Heymsfield SB, Caan BJ. Scaling of computed tomography body composition to height: relevance of height-normalized indices in patients with colorectal cancer. J Cachexia Sarcopenia Muscle 2022;13:203-9.
9. Dercle L, Zhao B, Gönen M, Moskowitz CS, Connors DE, Yang H, Lu L, Reidy-Lagunes D, Fojo T, Karovic S, Maitland ML, Oxnard GR, Schwartz LH. An imaging signature to predict outcome in metastatic colorectal cancer using routine computed tomography scans. Eur J Cancer 2022;161:138-47.
10. Kessner R, Sommer J, Große Hokamp N, Laukamp KR, Nayate A. Virtual versus true non-contrast images of the brain from spectral detector CT: comparison of attenuation values and image quality. Acta Radiol 2023;64:776-83.
11. Mingkwansook V, Puwametwongsa K, Watcharakorn A, Dechasasawat T. Comparative study of true and virtual non-contrast imaging generated from dual-layer spectral CT in patients with upper aerodigestive tract cancer. Pol J Radiol 2022;87:e678-87.
12. Ding Y, Richter A, Stiller W, Kauczor HU, Weber TF. Association between true non-contrast and virtual non-contrast vertebral bone CT attenuation values determined using dual-layer spectral detector CT. Eur J Radiol 2019;121:108740.
13. Mergen V, Racine D, Jungblut L, Sartoretti T, Bickel S, Monnin P, Higashigaito K, Martini K, Alkadhi H, Euler A. Virtual Noncontrast Abdominal Imaging with Photon-counting Detector CT. Radiology 2022;305:107-15.
14. Cao J, Lennartz S, Pisuchpen N, Parakh A, Kambadakone A. Attenuation values on virtual unenhanced images obtained with detector-based dual-energy computed tomography: observations on single- and split-bolus contrast protocols. Abdom Radiol (NY) 2022;47:3019-27.
15. Sauter AP, Muenzel D, Dangelmaier J, Braren R, Pfeiffer F, Rummeny EJ, Noël PB, Fingerle AA. Dual-layer spectral computed tomography: Virtual non-contrast in comparison to true non-contrast images. Eur J Radiol 2018;104:108-14.
16. Lennartz S, Parakh A, Cao J, Kambadakone A. Longitudinal reproducibility of attenuation measurements on virtual unenhanced images: multivendor dual-energy CT evaluation. Eur Radiol 2021;31:9240-9.
17. Azuma M, Nakada H, Khant ZA, Kimura A, Hirai T. Virtual Noncontrast Images Derived From Contrast-

Enhanced Dual-Layer Spectral Abdominal Computed Tomography: A Pilot Study Between Pediatric and Adult Scans. J Comput Assist Tomogr 2022;46:71-7.
18. Ma G, Han D, Dang S, Yu N, Yang Q, Yang C, Jin C, Dou Y. Replacing true unenhanced imaging in renal carcinoma with virtual unenhanced images in dual-energy spectral CT: a feasibility study. Clin Radiol 2021;76:81.e21-7.
19. Zhang X, Zhang G, Xu L, Bai X, Lu X, Yu S, Sun H, Jin Z. Utilisation of virtual non-contrast images and virtual mono-energetic images acquired from dual-layer spectral CT for renal cell carcinoma: image quality and radiation dose. Insights Imaging 2022;13:12.
20. Jing M, Sun J, Xi H, Liu Z, Zhang S, Deng L, Han T, Zhang B, Lin X, Zhou J. Abdominal virtual non-contrast images derived from energy spectrum CT to evaluate chemotherapy-related fatty liver disease. Quant Imaging Med Surg 2023;13:669-81.
21. Obmann MM, Kelsch V, Cosentino A, Hofmann V, Boll DT, Benz MR. Interscanner and Intrascanner Comparison of Virtual Unenhanced Attenuation Values Derived From Twin Beam Dual-Energy and Dual-Source, Dual-Energy Computed Tomography. Invest Radiol 2019;54:1-6.
22. Ananthakrishnan L, Rajiah P, Ahn R, Rassouli N, Xi Y, Soesbe TC, Lewis MA, Lenkinski RE, Leyendecker JR, Abbara S. Spectral detector CT-derived virtual non-contrast images: comparison of attenuation values with unenhanced CT. Abdom Radiol (NY) 2017;42:702-9.
23. Brady SL, Mirro AE, Moore BM, Kaufman RA. How to Appropriately Calculate Effective Dose for CT Using Either Size-Specific Dose Estimates or Dose-Length Product. AJR Am J Roentgenol 2015;204:953-8.
24. Lee MH, Park HJ, Kim JN, Kim MS, Hong SW, Park JH, Kang CH. Virtual non-contrast images from dual-energy CT angiography of the abdominal aorta and femoral arteries: comparison with true non-contrast CT images. Br J Radiol 2022;95:20220378.
25. Lennartz S, Laukamp KR, Tandon Y, Jordan M, Große Hokamp N, Zopfs D, Pennig L, Obmann M, Gilkeson RC, Herrmann KA, Ramaiya N, Gupta A. Abdominal vessel depiction on virtual triphasic spectral detector CT: initial clinical experience. Abdom Radiol (NY) 2021;46:3501-11.
26. Choi MH, Lee YJ, Choi YJ, Pak S. Dual-energy CT of the liver: True noncontrast vs. virtual noncontrast images derived from multiple phases for the diagnosis of fatty liver. Eur J Radiol 2021;140:109741.
27. Borhani AA, Kulzer M, Iranpour N, Ghodadra A, Sparrow M, Furlan A, Tublin ME. Comparison of true unenhanced and virtual unenhanced (VUE) attenuation values in abdominopelvic single-source rapid kilovoltage-switching spectral CT. Abdom Radiol (NY) 2017;42:710-7.
28. Jamali S, Michoux N, Coche E, Dragean CA. Virtual unenhanced phase with spectral dual-energy CT: Is it an alternative to conventional true unenhanced phase for abdominal tissues? Diagn Interv Imaging 2019;100:503-11.
29. Kazimierczak W, Kazimierczak N, Serafin Z. Quality of virtual-non-contrast phases derived from arterial and delayed phases of fast-kVp switching dual-energy CT in patients after endovascular aortic repair. Int J Cardiovasc Imaging 2023;39:1805-13.
30. Lehti L, Söderberg M, Höglund P, Wassélius J. Comparing Arterial- and Venous-Phase Acquisition for Optimization of Virtual Noncontrast Images From Dual-Energy Computed Tomography Angiography. J Comput Assist Tomogr 2019;43:770-4.

Cite this article as: Wen D, Pu Q, Peng P, Yue X, Ming Y, Yang H, Yang J, Zhang X, Liu H, Yang L, Sun J. Comparison of virtual and true non-contrast images from dual-layer spectral detector computed tomography (CT) in patients with colorectal cancer. Quant Imaging Med Surg 2024;14(9):6260-6272. doi: 10.21037/qims-24-535

